

Crystal growth in incongruently-melting compositions: programmed cooling experiments with diopside

R. JAMES KIRKPATRICK, LUNG-CHUAN KUO

*Department of Geology, University of Illinois
Urbana, Illinois 61801*

AND JOHN MELCHIOR

*Scripps Institution of Oceanography
La Jolla, California 92093*

Abstract

Programmed cooling experiments using a synthetic diopside glass and constant cooling rates of from 10° to 300°C/hr first crystallize forsterite and then with decreasing temperature clinopyroxene + wollastonite. The forsterite grows as hopper-shaped crystals which then develop dendrites from external corners. The morphological development can be qualitatively explained by a model involving diffusion in the melt and interface attachment kinetics. Microprobe traverses across forsterite-glass interfaces show that the magnitude of the MgO depletion in the melt near flat interface segments varies from 1.72 to 4.28 percent and increases with increasing run time for a given cooling rate and with increasing value of the product of the cooling rate times the run time for all cooling rates. The results are in qualitative agreement with theoretical predictions. Near a particular crystal MgO depletion is least at corners and greatest in reentrants. The clinopyroxene is more magnesian than diopside (solid solution towards enstatite) and grows as dendrites. The wollastonite occurs between the clinopyroxene dendrite arms. The clinopyroxene first appears at nominal undercoolings (1391 T_{quench}) of from 182° to 240°C, depending on the cooling rate. Unlike other sets of programmed cooling experiments which show a continual increase in nominal undercooling with increasing cooling rate, these experiments show a maximum in clinopyroxene undercooling at 50°C/hr. The undercooling is actually least for the 300°C/hr runs.

Introduction

When crystals grow from a melt with a different composition at least two processes must be involved in the growth process: the molecular attachment process occurring at the crystal-melt interface, and redistribution of chemical components in the melt in response to the selective removal of some of them by the crystal. Removal of the latent heat of crystallization from the crystal-melt interface may be important if the growth rate is high. Traditional descriptions of the interaction of diffusion and crystal growth assume that the liquid and crystal compositions at the interface are the equilibrium compositions for the temperature at which growth is occurring (e.g., Elbaum, 1959). Such descriptions may not be satisfactory for silicates and other materials which grow by a layer-spreading mechanism, because these

materials require a finite supersaturation or undercooling (really the same thing) at the interface for growth to occur (O'Hara *et al.*, 1968; Hopper and Uhlmann, 1974; Kirkpatrick, 1975). This layer-spreading growth mechanism also greatly affects the development of skeletal and dendritic crystal morphologies, allowing fully-faceted crystals to grow to a larger size than would be possible if interface kinetics were not important. Recent theoretical developments have shown how the effect of interface kinetics can be taken into account for both interface stability and the overall growth process.

This paper briefly reviews the recent theory, presents the results of programmed cooling experiments in which forsterite, clinopyroxene, and wollastonite grow from a synthetic stoichiometric diopside melt, and uses the theory to interpret these results.

Theory

Recent advances in crystal growth theory can help in the understanding of three major aspects of the experiments to be discussed here: (1) the origin of the skeletal morphologies of the forsterite and clinopyroxene crystals, (2) the time (temperature), position, and cooling rate dependences of the liquid composition at the forsterite–melt interface, and (3) the variation in liquid composition away from the forsterite–liquid interface. This section will briefly review these theoretical developments.

Interface stability

When a crystal is growing freely (*i.e.*, loss of latent heat through the melt) there is a tendency for the interface to break down into a cellular morphology. Theoretical analysis of this interface breakdown, taking into account surface energy and a continuous growth mechanism, indicates that planar interfaces on freely growing crystals larger than a few microns should be unstable (Elbaum, 1959; Mullins and Sekerka, 1963; see Lofgren, 1974, and Kirkpatrick, 1975, for reviews).

As noted by O'Hara *et al.* (1968) and many others since, this is clearly at variance with observation. There are many situations where cm-size or larger faceted crystals can be produced. The problem with the older calculations is that they neglect the stabilizing influence of layer-spreading growth mechanisms. These models correctly predict interface breakdown for low entropy of fusion materials like metals, which do not grow by layer spreading, but apparently do not apply to high entropy of fusion materials like silicates (Jackson, 1958).

The interface stability of high entropy of fusion materials has been discussed by Cahn (1967), Tarshis and Tiller (1967), O'Hara *et al.* (1968), Chernov (1974), and Lawrence and Elwell (1976). Of these, Chernov's analysis is the most complete and will be followed here.

Chernov has recognized three ways a faceted crystal may evolve into a non-faceted habit. These are: (1) random fluctuations on a flat interface, (2) random fluctuations at edges or corners, and (3) what we will call macroscopic diffusional instability. For all three, growth by a layer-spreading mechanism enhances the morphological stability. For materials which grow by layer-spreading mechanisms, such as most silicates, it appears that interface breakdown should occur by random fluctuations at corners or macroscopic diffusional instability.

The fundamental reason that layer-spreading growth enhances morphological stability is that the spacing between the steps on the surface can change with changing local undercooling or supersaturation in such a way that the growth rate of the face remains constant. If the undercooling is greater at one location, the spacing increases; if the undercooling is less, the spacing decreases. In this way the face can continue propagating parallel to itself, although the average slope of the interface with respect to the ideal crystallographic surface will change slightly. According to Chernov (1974), slopes of about 1° can compensate for inhomogeneities in the interface melt composition of about 20 percent for moderately effective layer-spreading growth.

Chernov's analysis of instability by random fluctuations on flat interfaces indicates that growth by a layer-spreading mechanism is very effective at stabilizing the interface. When growth is by the continuous mechanism any protuberance from a freely growing crystal will see a larger undercooling and will grow more rapidly, causing the crystal to grow with a cellular morphology. For a crystal growing by a layer-spreading mechanism this effect is counteracted by the sideways growth of the steps. Thus, as a protuberance develops and the local slope increases, the protuberance generates many surface steps which move rapidly away, eliminating the irregularity from the surface.

The other two ways faceted crystals may break down are associated with corners and edges. Of these, macroscopic diffusional instability leads to hopper-shaped crystals, and random fluctuation leads to dendrite growth from corners or edges. Both of these are common morphologies of silicate and oxide crystals in igneous rocks and in the experiments discussed in this paper.

Macroscopic diffusional instability occurs when the decrease in the spacing of the growth steps on the surface with decreasing local supersaturation can no longer compensate for variations in the supersaturation along the interface. When this happens growth stops or slows drastically in areas of low supersaturation. In most cases the low supersaturation occurs in the center of a face because there is a much lower volume of melt per unit area of interface at the center than there is at the corners. Lateral diffusion parallel to the face helps eliminate this inhomogeneity, but as the crystal grows larger it becomes less effective.

The result of macroscopic diffusional instability is a hopper crystal. In some cases only the fastest-grow-

ing face of a crystal becomes hopper-shaped, while the more slowly-growing faces remain planar. This results in a hopper crystal with some planar faces. If there are other crystallographic planes on which growth can occur at high angles to the one breaking down, faceted macrosteps may develop. This leads to kinematic waves which pass over the surface with growth taking place at any particular place only when the macrostep passes over. Chernov's analysis indicates that this general kind of instability should be common in silicate systems.

Chernov's analysis of interface instability by random fluctuations at corners has not been carried as far, but his results indicate that, for crystals which grow by layer spreading, instability by fluctuations at corners or edges should be much more common than instability by fluctuation on flat faces. His analysis indicates that even if a fluctuation does not develop into a dendrite it may still result in a macrostep which will pass over the interface.

Instability spacing

In the traditional models the spacing (X) between dendrite arms is proportional to the ratio of the diffusion coefficient (D) in the melt to the growth rate (Y) ($X \propto D/Y$; Keith and Padden, 1963). In Chernov's analysis the transition to hopper morphology is directly related to the efficiency of diffusion in the melt parallel to the interface. The critical crystal size for onset of hopper growth is related to the ratio of the diffusion coefficient in the melt to the kinetic coefficient for growth times a number of system constants. The kinetic coefficient, b , is given by

$$Y = b\Delta T$$

where ΔT is the undercooling and Y is the growth rate.

Traditional models may be sufficient to describe secondary dendrites (those growing on existing dendrites) because the surfaces bounding many dendrite arms appear to be rounded and probably grow by a continuous mechanism.

Whether the spacing between primary dendrite arms growing from corners is also related to D/Y is not clear. The process has not, to our knowledge, been analyzed in sufficient detail to determine if there is a critical initiation size.

Interface melt composition

As for interface stability, the growth of crystals by layer-spreading mechanisms complicates the interpretation of composition gradients near growing

crystals. One of the few analyses of this problem which include interface kinetics is that of Hopper and Uhlmann (1974). Their calculations indicate that the concentration of the rejected component in the melt at the interface, the composition gradient in the melt at the interface, and the difference between the interface melt composition and the melt composition far from the interface all increase monotonically with increasing time. Their results can only be used as a general guide for interpreting the results of the experiments discussed here because they assume a constant temperature, growth rate, and diffusion coefficient.

Calculations more directly applicable to our experiments, although still difficult to apply quantitatively, are those of Ghez and Lew (1973) and Müller-Krumbhaar (1975). Both conclude that for samples cooled at a constant rate the supersaturation at the interface increases with increasing time, the same as Hopper and Uhlmann (1974). Müller-Krumbhaar indicates that for a given starting material the interface melt composition for all cooling rates should fall along one curve when plotted vs. the product of cooling rate, run-time, and some system constants. It is difficult to use the Müller-Krumbhaar relationships quantitatively because the activation energy for crystal growth and the temperature and composition dependences of the diffusion coefficients are unknown and because a simple first-power relationship between growth rate and supersaturation is assumed. In the absence of known phase relationships it is also difficult to distinguish this relationship from the equilibrium relationship, because cooling rate times run time is simply temperature.

Composition gradients in the melt

The need for transport of components to and from the crystal surface leads to composition gradients in the melt near the surface. For a binary system the component enriched in the crystal is depleted in the melt near the crystal and the rejected component is enriched.

For a multicomponent system the diffusion coefficient is not a single number but a matrix. The problem of a three-component system has been treated for the interface equilibrium, isothermal case by Cooper and Gupta (1971). Their results indicate that except in the most unusual situations the composition gradient will follow a curved path in composition space with only the mean composition of the liquid lying on the depletion line. Quantitatively their results are not applicable to the experiments dis-

cussed here because they assume constant diffusion coefficients. However, the results should be qualitatively the same for programmed cooling experiments.

Experiments

Procedure

Our experiments used programmed cooling methods with the samples held on platinum wire loops (Lofgren *et al.*, 1974). The starting material was synthetic stoichiometric diopside ($\text{CaMgSi}_2\text{O}_6$) glass for which crystal growth rates have been measured at both large and small undercoolings (Kirkpatrick, 1974; Kirkpatrick *et al.*, 1976). An experimental charge was made by pressing about 100 mg of powdered glass into a pellet and sintering the pellet onto a platinum wire loop. Each run was started by placing a charge in a MoSi_2 resistance furnace in the air at 1400°C (9°C above the liquidus temperature) for ten minutes. It was then cooled at a constant rate of from 10° to 300°C/hr . The thermocouples were calibrated against the melting points of gold and diopside. A number of samples were run at each cooling rate but quenched at different temperatures in order to observe the changes in mineralogy, composition, and texture as crystallization proceeds. The final product is a bead approximately 4 mm in diameter with varying amounts of glass and crystal.

The samples have been examined both whole and in polished thin section. Whole samples were examined primarily by petrographic microscope while immersed in oil of $n \cong 1.64$ with the sample held in a piece of copper tubing epoxied to a glass slide. This technique eliminated the lens effect of the glass bead, allowed the size and number of crystals in partially-crystallized samples to be determined, and permitted us to decide how to cut the sample. The partially-crystallized samples were then cast in epoxy and cut into several slices by a diamond saw with a $250\text{-}\mu\text{m}$ -thick blade such that a crystal or crystals were cut in a predetermined way. Some crystals were cut lengthwise; others were cut into serial slices about $250\ \mu\text{m}$ thick. These slices were then mounted as either thin ($30\ \mu\text{m}$) or thick sections. The fully-crystallized samples were cut in half and examined in thin section.

Analytical methods

Quantitative analyses of the glass, forsterite, and clinopyroxene were made with an ARL-EMX electron microprobe. The beam current was approximately 0.07 microamps, the accelerating voltage 20 kV, and

the beam diameter $1\ \mu\text{m}$. The standard was a synthetic diopside glass. Drift, background, and dead-time corrections were made with the computer program PROBE. Absorption, fluorescence, backscatter, and stopping power corrections were made with a modified version of the program ABFAN (Boyd *et al.*, 1969).

The composition gradients in the glass near crystals were measured by first running qualitative profiles along the desired traverse with a JEOL JXA-50A electron microprobe at a scan speed of $40\ \mu\text{m}$ per minute and then calibrating the scans with three to eight quantitative analyses along the traverse. The glass compositions at the crystal-glass interface were obtained by extrapolating the calibrated scans. In almost all cases there is an analysis within $15\ \mu\text{m}$ of the interface, and extrapolation is never large.

Because the smallest grains in the fully crystallized charges are 1 to $5\ \mu\text{m}$ across, several of these charges were powdered and X-rayed on a Norelco powder diffractometer at $1^\circ\ 2\theta$ per minute with Ni-filtered $\text{CuK}\alpha$ radiation. Phase identification was made from the ASTM powder file.

Results

The phases occurring in these experiments are glass, forsterite, a clinopyroxene, and wollastonite. Figure 1 is a plot of temperature, run time, and phases present for each run. At nominal undercoolings (1391°C -quench temperature) less than about 140° to 160°C depending on the cooling rate, the only phase is glass. At somewhat larger nominal undercoolings, up to 240° , only glass plus less than 5 percent hopper or dendritic forsterite are present. At the largest undercoolings the samples appear to be fully crystallized and contain mostly dendritic clinopyroxene crystals with a small amount of wollastonite in the interstices between the clinopyroxene dendrite arms, along with the previously-crystallized forsterite.

For cooling rates less than 50°C/hr the temperature of first appearance of clinopyroxene and wollastonite decreases with increasing cooling rate. This is similar to the variation observed in all previous sets of programmed cooling experiments (see, for instance, Walker *et al.*, 1976; Grove and Raudsepp, 1978). At larger cooling rates (100° to 300°C/hr), however, the temperature of first appearance of clinopyroxene and wollastonite increases (the nominal undercooling decreases). This is opposite the previously-observed variation. The variation in the tem-

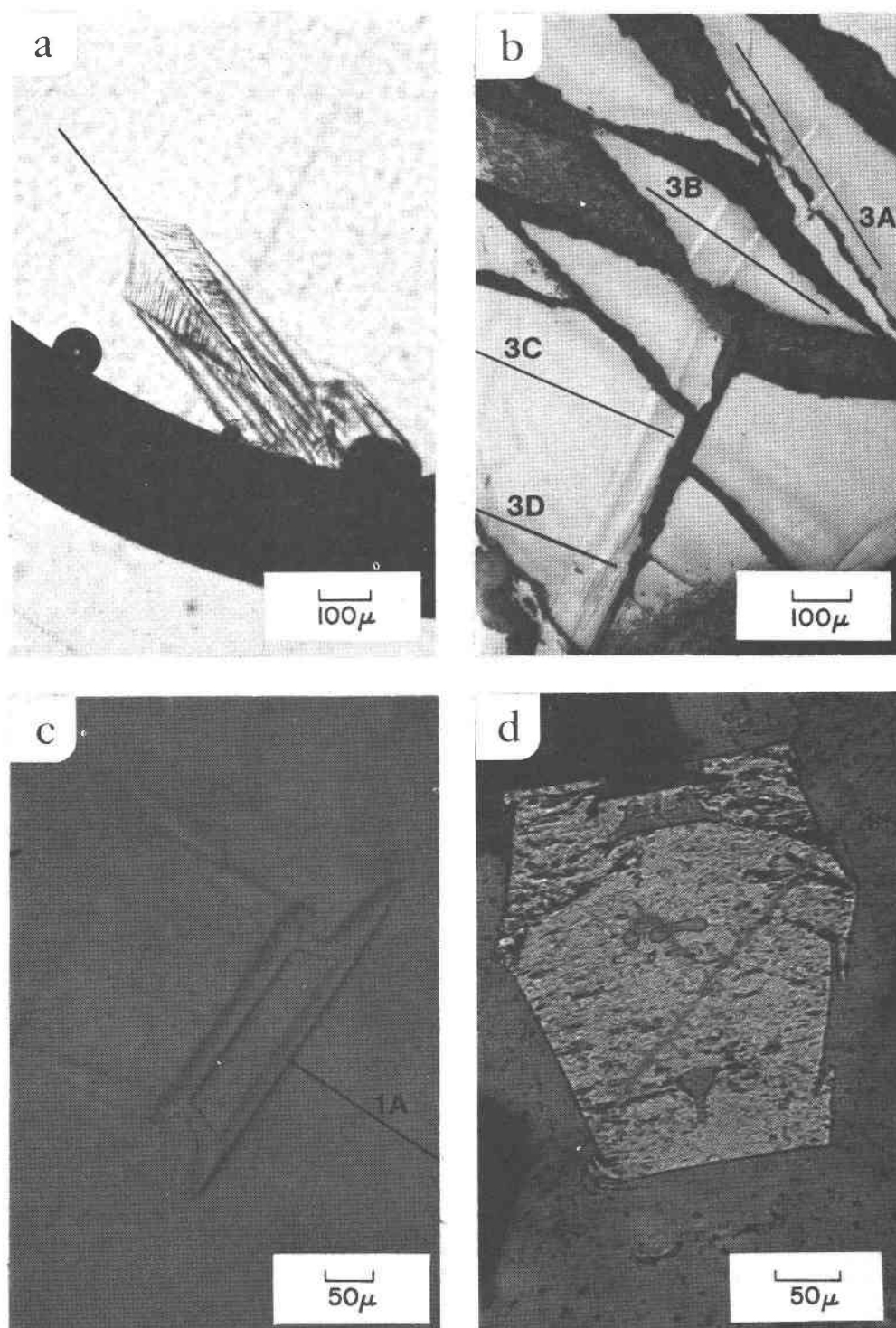


Fig. 2. Photomicrographs of olivine crystals. (a) Hopper-shaped experimental forsterite nucleating on wire loop. Electron microprobe scan along solid line is shown in Fig. 10. Striations on crystal are macrosteps on inside of hopper. $10^\circ/\text{hr}$, $T_q = 1214^\circ\text{C}$. Plane transmitted light. (b) Hopper-shaped experimental forsterite crystal. Electron microprobe scans were done along transverses 3A to 3D. MgO depletion (ΔMgO) increases from 2.94 wt% near top to 3.68 wt% near base (lower left). $50^\circ/\text{hr}$, $T_q = 1177^\circ\text{C}$. Plane reflected light. (c) Hopper-shaped experimental forsterite crystal with dendrite arms developing at corners or external hoppers. Plane reflected light. $100^\circ/\text{hr}$, $T_q = 1186^\circ\text{C}$. (d) Olivine phenocryst in mid-Atlantic ridge basalt. Note development of dendrite arms from corners, melt inclusions, and kinematic wave on lower right corner. Surfaces are curved, indicating a high step density. Plane transmitted light.

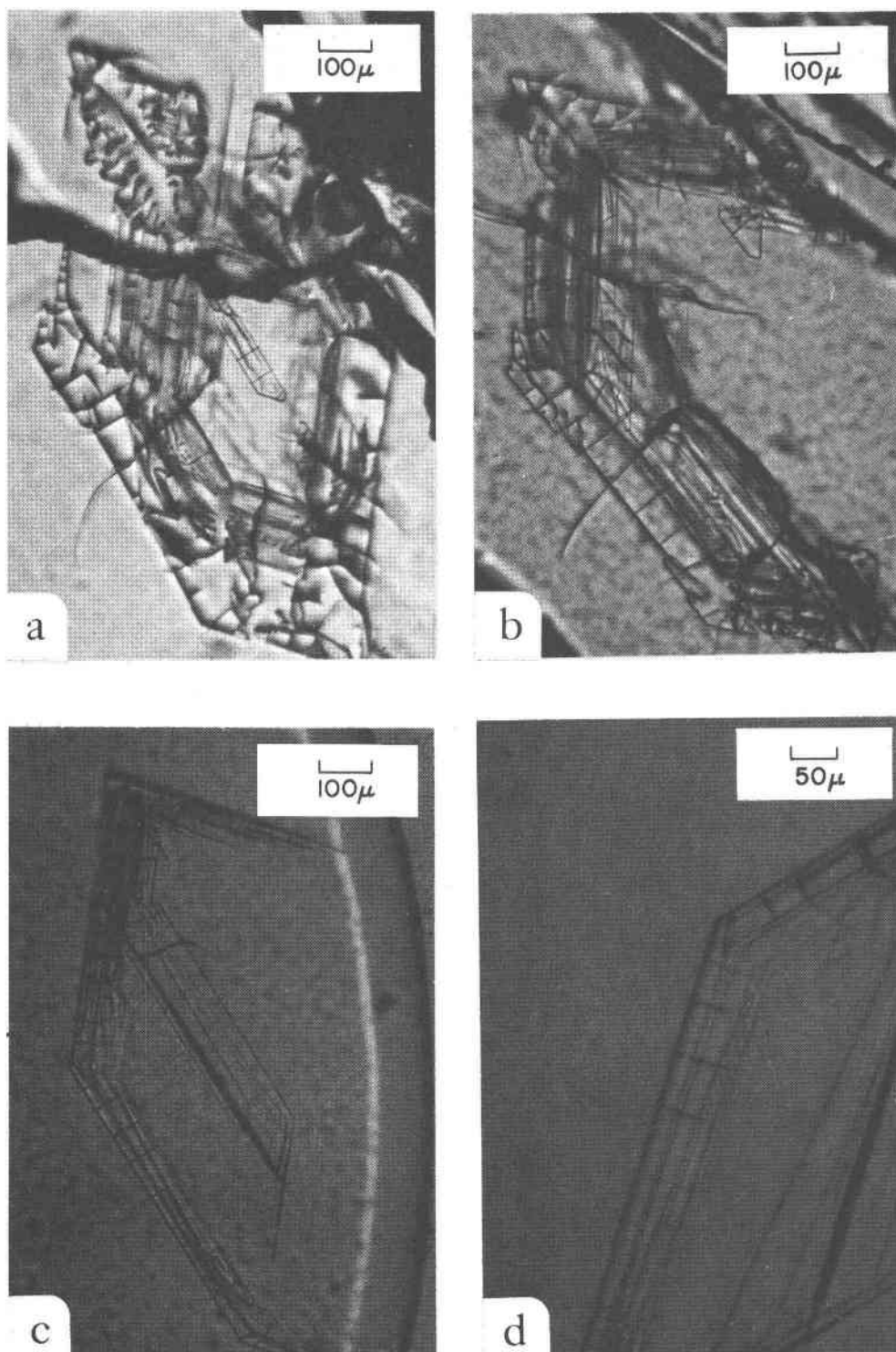


Fig. 3. Photomicrographs of serial sections through a hopper-shaped and dendritic experimental forsterite crystal, $10^\circ/\text{hr}$, $T_q = 1201^\circ\text{C}$. Plane transmitted light. (a) Slice $500\ \mu\text{m}$ from base of crystal showing extensive dendrite development. (b) Slice $500\ \mu\text{m}$ from that in 3a, showing less well developed dendrites. (c) Slice $500\ \mu\text{m}$ from that in 3b and about $250\ \mu\text{m}$ from the end of the crystal showing hopper development, but a mostly faceted external morphology. (d) Close-up of slice in Figure 3c showing mostly flat crystal surfaces with a kinematic wave starting at the corner.

Table 3. (cont.)

	Run 56A							
	1	2	3	4	5	6	7	8
CaO	27.51	27.30	27.18	27.34	27.08	26.69	26.43	26.44
SiO ₂	56.94	55.95	56.64	55.22	55.10	55.41	54.89	55.37
MgO	15.76	15.78	15.95	16.64	17.15	17.67	18.28	17.97
Total	100.21	99.03	99.77	99.20	99.33	99.77	99.60	99.78
Ca	1.060	1.066	1.051	1.069	1.057	1.036	1.028	1.025
Si	2.048	2.038	2.045	2.013	2.006	2.006	1.992	2.003
Mg	0.845	0.857	0.858	0.904	0.930	0.953	0.989	0.969
O	6.000	6.000	6.000	6.000	6.000	6.000	6.000	6.000

forsterite (with about 1% CaO) depletion line, but are curved. The melt near the crystal is enriched in SiO₂ relative to forsterite depletion. Going away from the interface the gradients cross or come to the forsterite depletion line and then curve towards the original diopside bulk composition. Even the most MgO-de-

pleted compositions at the interface are still well within the diopside primary phase field.

The MgO value in the glass at the interface and Δ MgO vary systematically with location on the interface, run time at a given cooling rate, and the product of run time and cooling rate for all the cooling

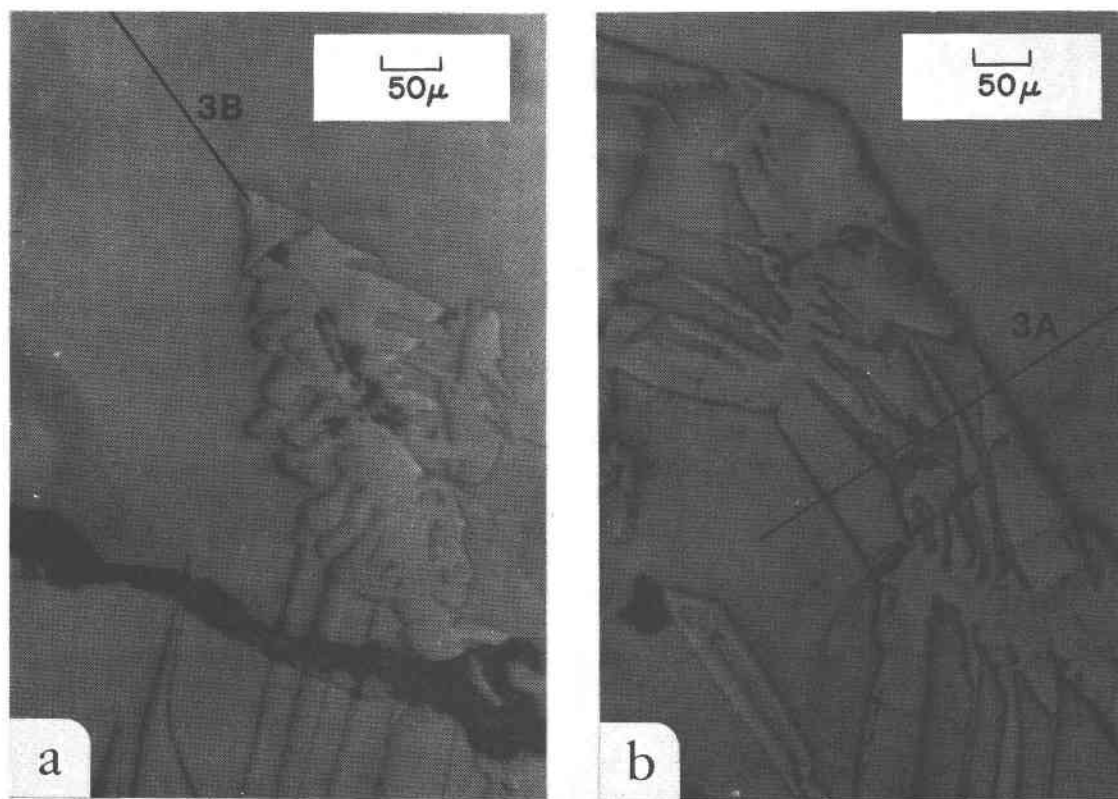


Fig. 4. Close-up plane reflected light photomicrographs of the slice shown in Fig. 3a. (a) Dendrite arm showing nonfaceted secondary arms (except on a few external surfaces) and entrapment of melt by secondary arms growing from bottom. (b) Dendrite arms showing entrapment of melt by growth of secondary dendrites perpendicular to overall growth direction, non-planar internal surfaces and planar external surfaces.

Table 4. Glass compositions in forsterite plus glass runs

Run No.	Cooling rate (°/hr)	T _{quench} (°C)	Scan No.	C [∞]		C _i		C [∞] -C _i		Interface position*
				CaO	MgO	CaO	MgO	ΔCaO	ΔMgO	
55A	200	1186	1A	26.22	18.29	27.50	14.99	-1.28	3.30	F
			1B	26.12	18.20	27.52	14.61	-1.40	3.59	F
			1C	26.16	18.46	27.46	15.40	-1.30	3.06	F
			2A	26.30	18.50	27.30	15.68	-1.00	2.82	F
			2B	26.10	18.07	27.61	15.10	-1.51	2.97	F
			2D	26.20	17.98	27.14	15.12	-0.94	2.86	F
43A	100	1211	1A	26.72	18.06	27.47	15.86	-0.75	2.20	F
44A	100	1191	3A	26.04	18.00	27.57	13.74	-1.53	4.26	F
			3B	25.89	18.16	27.53	13.88	-1.64	4.28	F
			3C	25.75	17.92	27.30	13.96	-1.55	3.96	F
			3D	26.10	18.00	27.48	14.04	-1.38	3.96	F
52A	100	1186	1A	26.91	18.18	27.90	15.36	-0.99	2.82	F
47A	50	1177	1B	27.38	18.00	28.40	14.62	-1.02	3.38	F
			3A	27.50	18.02	28.64	15.08	-1.14	2.94	D
			3B	27.51	17.82	28.66	14.71	-1.15	3.11	F
			3C	27.32	17.64	28.50	14.28	-1.18	3.36	F
			3D	27.50	17.72	28.76	14.04	-1.26	3.68	F
66A	50	1158	1B	26.76	18.00	28.26	14.38	-1.40	3.62	F
			2A	26.75	18.52	28.60	14.56	-1.85	3.96	F
			2B	26.70	18.42	28.02	14.62	-1.32	3.80	F
			2C	26.50	18.30	28.15	14.56	-1.65	3.74	F
78A	50	1152	3A	26.67	17.82	28.50	13.96	-1.83	3.86	D
			3B	26.66	18.00	28.60	13.90	-1.94	4.10	F
			3C	26.52	17.76	28.58	13.52	-2.06	4.24	R
			3D	26.50	18.00	28.22	13.88	-1.72	4.12	F
			6A	26.30	18.00	28.18	14.12	-1.88	3.88	D
			6C	26.18	18.25	28.20	14.16	-2.02	4.09	F
65A	20	1171	2A	26.48	17.06	27.52	14.48	-1.04	2.58	F
			3B	26.22	16.48	27.23	13.48	-1.01	3.00	F
75A	20	1162	3A	26.50	17.42	27.68	14.00	-1.18	3.42	F
			3B	26.58	17.30	27.70	13.78	-1.12	3.52	R
			4A	26.52	17.24	27.94	14.13	-1.42	3.11	F
			4B	26.30	17.08	27.78	13.76	-1.48	3.32	R
			5A	26.52	17.38	27.82	14.10	-1.30	3.28	F
			5B	26.48	17.40	27.76	13.84	-1.28	3.56	R
			6A	26.50	17.00	27.78	13.62	-1.28	3.38	F
			6B	26.48	17.03	27.86	13.36	-1.38	3.67	R
45A	10	1235	2A	26.50	18.00	27.36	16.20	-0.86	1.80	F
			2B	26.40	18.06	27.30	16.32	-0.90	1.74	F
49A	10	1225	3A	26.68	18.60	27.72	16.57	-1.04	2.03	F
			3B	26.28	18.50	27.18	16.78	-0.90	1.72	D
			3C	26.26	18.48	27.28	16.52	-1.02	1.96	F
56A	10	1214	2A	26.50	18.06	27.60	15.98	-1.10	2.08	F
57A	10	1201	1A	27.18	17.73	28.30	15.53	-1.12	2.20	F
			1B	26.97	17.69	28.30	15.18	-1.33	2.51	R
			2A	26.76	17.48	28.13	15.06	-1.37	2.42	F
			2B	27.01	17.74	28.10	15.90	-1.09	1.84	D
			3A	26.66	17.50	28.08	15.02	-1.42	2.48	F
			3B	26.80	17.30	27.82	15.56	-1.02	1.74	D

*Interface position: F = flat, R = reentrant, D = dendritic tip or corner

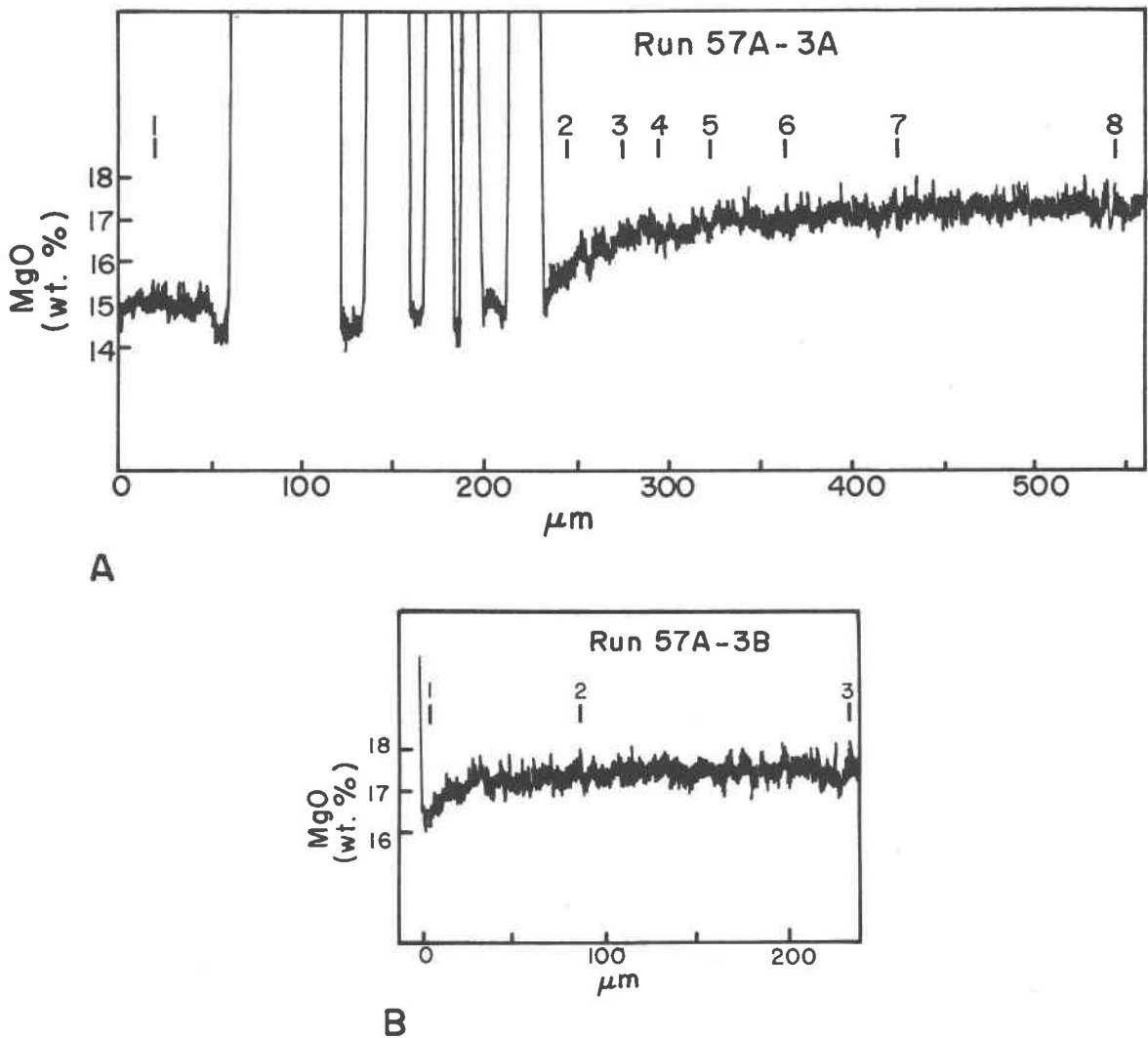


Fig. 5. Calibrated electron microprobe scans showing the MgO gradients in the glass near forsterite crystals. Off-scale peaks are crystal. Both scans are for same crystal. 57A-3A is across a flat interface segment; 57A-3B is across a dendrite tip (see Fig. 4). Low MgO values on the left side of 57A-3A scan are melt inclusions. Note even lower MgO than at the interface.

rates. These variations are in good agreement with the theory discussed above.

The data in Table 4 indicate that the nature of the interface greatly influences the interface composition. Relative to the composition next to flat interface segments, ΔMgO near dendrites or corners (those parts of the crystal protruding into the melt) is lower and MgO at the interface is higher. At reentrants, on the other hand, ΔMgO is greater and MgO at the interface is lower. Because of this we use only data from flat interface segments to compare data from different runs.

For runs done at the same cooling rate but for different lengths of time ΔMgO increases and MgO at the interface decreases with increasing run time. Figure 8 shows this variation for runs at 50° and 10°C/hr.

Figure 9 shows the ratio of MgO at the interface to MgO in the bulk melt vs. the product of cooling rate and run time. This plot allows comparison with theoretical prediction (Müller-Krumbhaar, 1975). MgO at the interface would show the same decrease, and ΔMgO would increase. Almost all the MgO ratios plot on the same convex-upward curve. The one

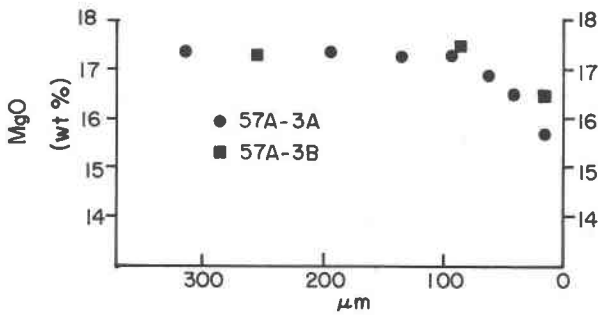


Fig. 6. Electron microprobe analyses (MgO) vs. position used to calibrate scans in Fig. 5.

crystal (3 data points) at $100^{\circ}\text{C}/\text{hr}$ that does not is much larger than other crystals at the same cooling rate and may have nucleated at a higher temperature. The other data at this cooling rate fall on the overall trend.

A number of forsterite crystals contain numerous melt inclusions trapped between dendrite arms. Table 3 and Figure 5a present analyses of the inclusions in the sample illustrated in Figures 3a and 4. The inclusion compositions are somewhat scattered but are all significantly lower in MgO (forsterite) than even the glass composition at the external interface. This is probably due to continued growth of forsterite onto the inclusion wall after it was trapped. The inclusion compositions are poor estimates of the bulk liquid composition from which the crystals are

growing, a conclusion also reached by Roedder and Weiblen (1977) for lunar mare basalts.

Figure 10 presents a calibrated microprobe scan down the axis of the hopper crystal illustrated in Figure 2a. Table 3 gives the analyses used to calibrate this scan. The continual decrease in MgO from the mouth of the hopper to its base also indicates continual growth on the inside of the crystal.

The partitioning of Ca and Mg between the melt and olivine shows no systematic temperature or cooling rate dependence, and the olivine is much richer in calcium than the equilibrium value predicted by extrapolating the data of Watson (1979) for experiments in the system $\text{Na}_2\text{O}-\text{CaO}-\text{MgO}-\text{Al}_2\text{O}_3-\text{SiO}_2$. Figure 11 shows the olivine-liquid partition coefficients, $(\text{CaO}/\text{MgO})_{\text{ol}}/(\text{CaO}/\text{MgO})_{\text{liq}}$, using the extrapolated interface liquid compositions at flat interface segments plotted vs. $1/T^{\circ}\text{K}$, along with Watson's equilibrium data. Care was taken not to analyze the forsterite within about $15\ \mu\text{m}$ of the interface because of secondary fluorescence effects. Similarly, there is no systematic variation when the partition coefficients are plotted vs. cooling rate. Indeed, the data for one crystal at $10^4/T^{\circ}\text{K} = 6.83$ in Figure 11 span nearly the entire range. All the partition coefficients from the programmed cooling experiments are much larger than the equilibrium values of Watson. This reflects the much higher CaO values in our olivines (0.71 to 1.43 wt%, Table 1) relative to his (0.03 to 0.53 wt%).

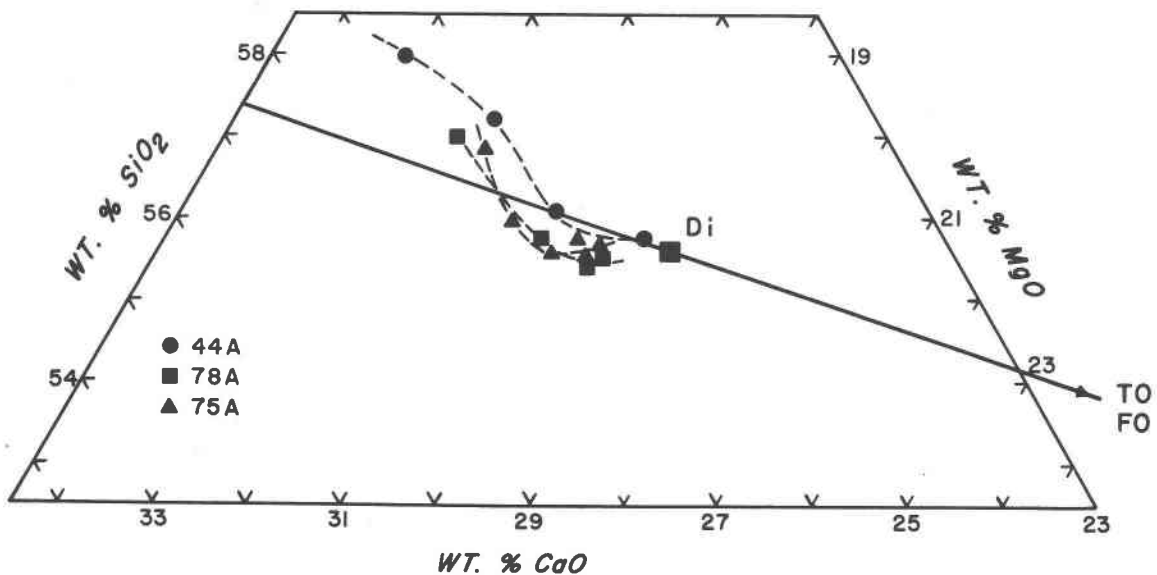


Fig. 7. Composition gradients in glass close to forsterite crystals plotted in the system $\text{CaO}-\text{MgO}-\text{SiO}_2$. Points near the diopside composition are far from the interface; points away from the diopside composition are next to forsterite crystals. The curvature of the gradients in composition space is in agreement with the theory of Cooper and Gupta (1971) and is due to multicomponent diffusion effects.

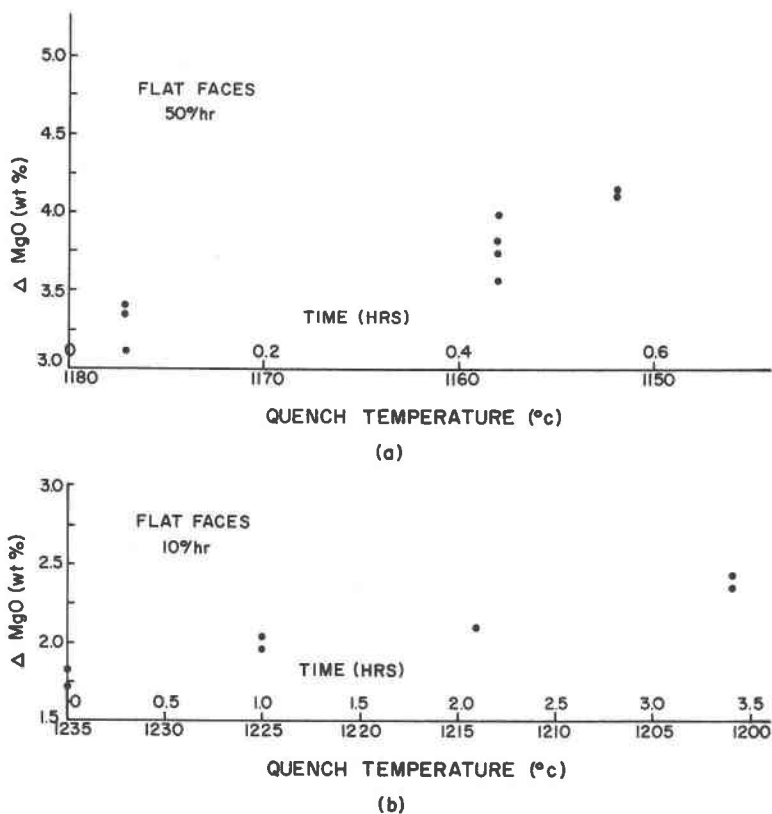


Fig. 8. ΔMgO vs. time for flat interface segments: (a) 50°/hr; (b) 10°/hr.

Clinopyroxene and wollastonite

A clinopyroxene ($\text{Wo}_{47}\text{--}\text{Wo}_{49}$) and wollastonite crystallize after forsterite, beginning at temperatures ranging from 1209° to 1151°C, depending on cooling rate. There is a minimum in the appearance temperature at a cooling rate of 50°C/hr (Fig. 1). No glass can be seen in thin sections of any run containing clinopyroxene and wollastonite.

The clinopyroxene crystals are all dendritic, with as many as three levels of branching. The surfaces of the dendrites are rounded and appear to be non-crystallographic. There are from 2 to 13 clinopyroxene crystals in each thin section. The wollastonite crystals are located between the clinopyroxene dendrite arms, often in optically continuous networks. The more rapidly-cooled samples are often highly vesicular. Figure 12 illustrates typical clinopyroxene and wollastonite morphologies.

The clinopyroxene compositions are more magnesian than diopside and fall along the diopside–enstatite join. Table 5 lists typical electron microprobe analyses of the clinopyroxene. Figure 13 plots the analyses in the forsterite–wollastonite–silica system.

There appears to be no systematic variation of clinopyroxene composition with cooling rate or temperature. The wollastonite grains are too small to analyze with the microprobe.

It has been suggested (Kirkpatrick, 1975; Walker *et al.*, 1976; Grove and Walker, 1977) that dendrite arm spacing decreases with increasing undercooling (higher growth rate) and that the spacing may be

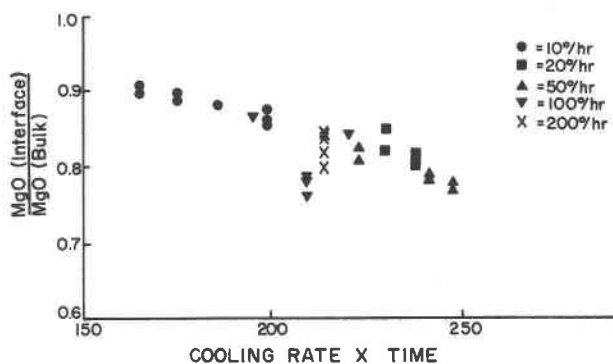


Fig. 9. $\text{MgO (interface)/MgO (bulk)}$ vs. cooling rate times run time for all flat interface segments examined. 100°/hr data that fall below trend are from unusually large crystal.

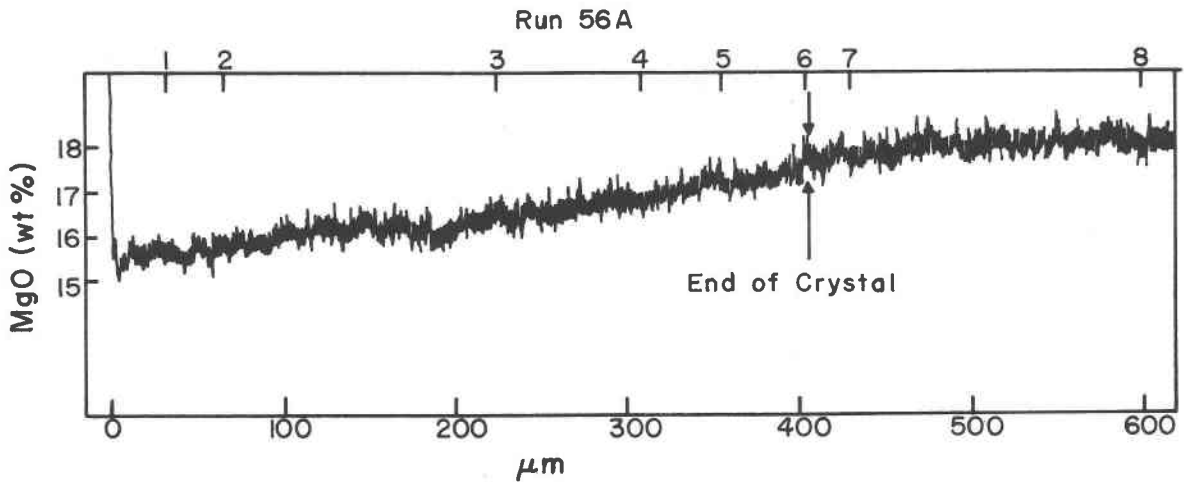


Fig. 10. Calibrated scan (MgO) of glass down the length of a hopper forsterite. Calibration points are given in Table 3, crystal is illustrated in Fig. 2a.

used as a measure of relative cooling rate. In our experiments the relationship between the temperature of crystallization and the spacing is poor. Figure 14 is a plot of the spacing of the finest-scale dendrites vs. cooling rate. These spacings were measured by rotating the thin section on a universal stage until the

arms were most clearly resolved and the spacing was a minimum. Although there is considerable scatter, it is clear that the spacings are the largest (about 10 μm) at the slowest cooling rates, have a minimum of about 4 μm in the range 50° to 200°C/hr, and increase slightly to about 6 μm in the 300°C/hr runs. The scatter in the data is real and not analytical. There are patches of different spacing, even within a single crystal. This variation in spacing may be due to variation in melt composition (and therefore liquidus temperature and therefore undercooling) associated with the composition gradients near forsterite crystals. We have not, however, been able to associate any changes with any specific forsterite crystals.

As for the forsterite, it is not possible to determine accurate nucleation or growth rates for the clinopyroxene. Because the crystals must have grown entirely between the run time of the longest run which contains only forsterite and glass and the run time of the shortest run which contains clinopyroxene, it is possible to estimate minimum average growth rates. For the 300°C/hr runs the crystals must have grown about 4 mm in less than 1 minute, so the growth rate must have been greater than about 7×10^{-3} cm/sec. For the 10°C/hr runs they must have grown about 4 mm in less than 18 minutes, so the growth rate must have been greater than about 4×10^{-4} cm/sec. These rates are in good agreement with growth rates of the order of 10^{-2} cm/sec for this bulk composition obtained in this temperature range from microscope heating-stage experiments (Kirkpatrick *et al.*, 1976). Because the samples are fully crystallized, it is not possible to determine the crystallographic direction with the highest growth rate.

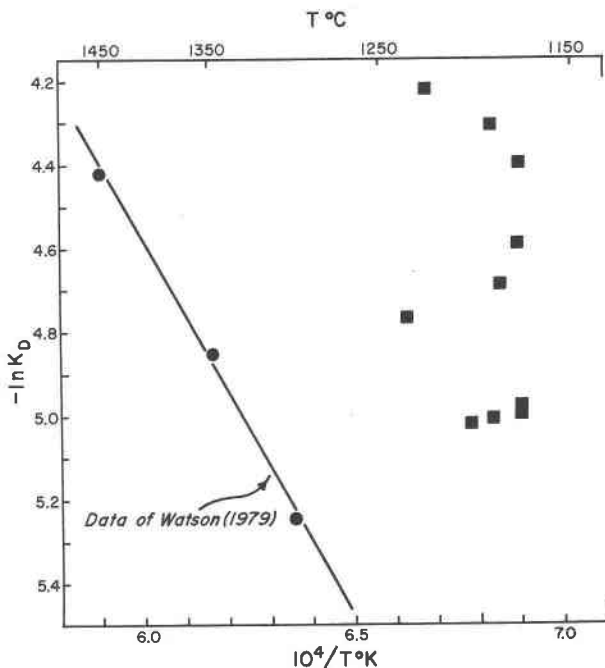


Fig. 11. Olivine-liquid partition coefficients, $K_D = (\text{CaO}/\text{MgO})_o/(\text{CaO}/\text{MgO})_{liq}$, using the extrapolated interface liquid compositions for the programmed cooling experiments (squares) along with the equilibrium values of Watson (1979) for experiments in the system $\text{Na}_2\text{O}-\text{CaO}-\text{MgO}-\text{Al}_2\text{O}_3-\text{SiO}_2$.

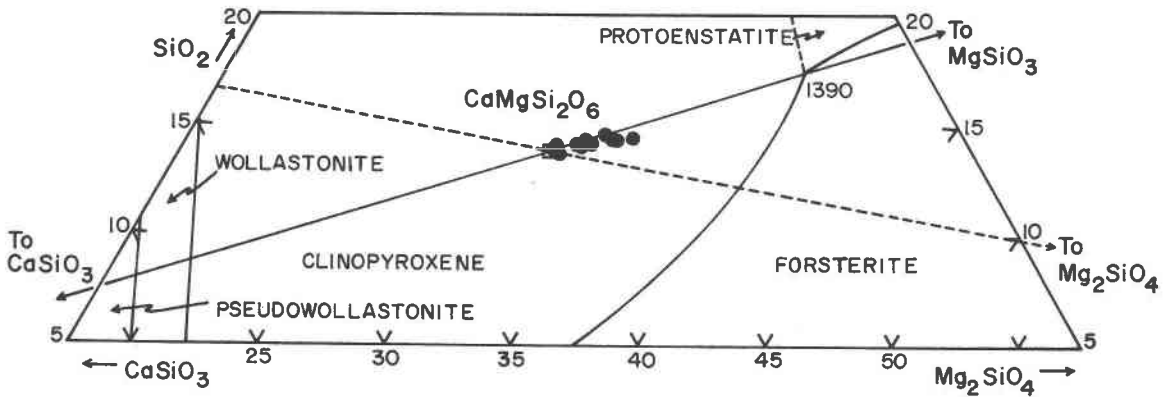


Fig. 13. Clinopyroxene compositions plotted in part of the system $\text{SiO}_2\text{-CaSiO}_3\text{-Mg}_2\text{SiO}_4$.

extrapolation is difficult to determine, but forsterite may be supercooled a few degrees. This result is in good agreement with other programmed cooling experiments using platinum loop methods (Donaldson *et al.*, 1975).

Similar metastable occurrence of olivine in programmed cooling experiments has been observed by Walker *et al.* (1978) for a eucritic meteorite composition almost on the olivine-liquid peritectic point. In their experiments, however, olivine always coexists with pyroxene.

Forsterite morphology

The development of the forsterite morphologies in these experiments is in very good agreement with the

predictions of the theory of Chernov (1974). The fundamental shape of almost all of the forsterite crystals is a hopper. Only a few of the thinnest crystals show a fully-faceted morphology, and this may be an accident of the way they were cut during sample preparation. The smallest crystals are usually hopper-shaped with some planar surfaces (Fig. 2a). Most of the larger ones are hopper-shaped with dendrite arms developed from corners. There is no evidence of breakdown of flat interfaces by random fluctuations. This implies that the forsterite is growing by a layer-spreading mechanism, that significant supersaturation at the interface is necessary to drive crystal growth, and that models which assume interface equilibrium will be insufficient to describe the growth.

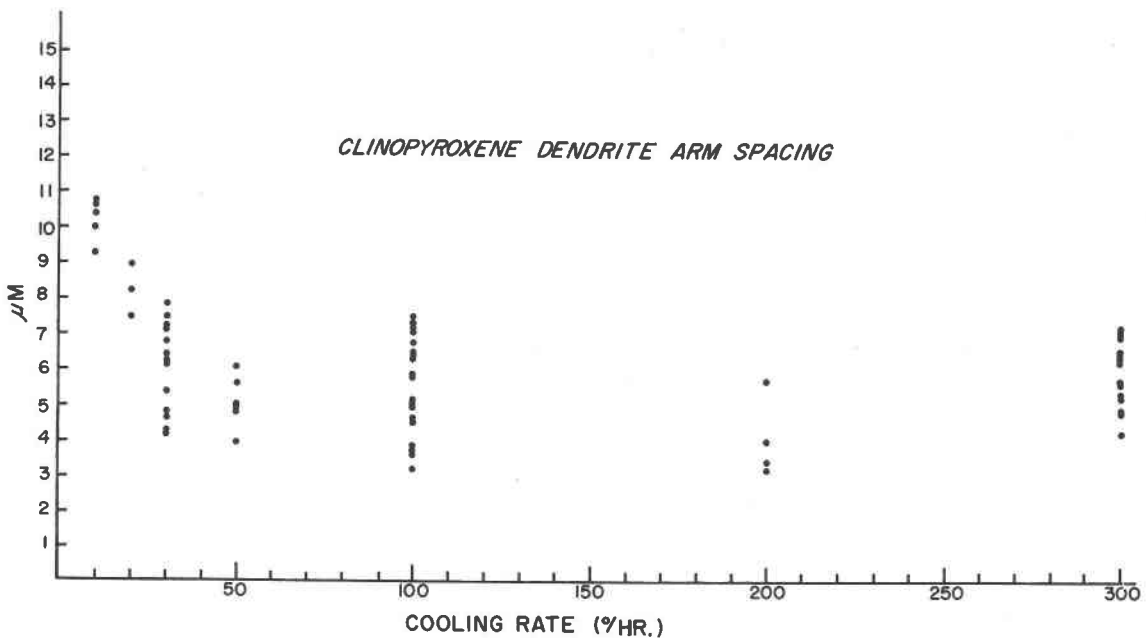


Fig. 14. Clinopyroxene dendrite arm spacing vs. cooling rate for all fully-crystallized runs.

It appears that breakdown of a euhedral forsterite crystal takes place first by macroscopic diffusional instability and only later by random fluctuations at corners. The critical crystal size for the onset of hopper morphology appears to be about 12 μm . This is probably small enough to be affected by surface energy (capillarity), although this still needs to be considered in the theoretical analysis. There appears to be no critical size for the onset of dendrite development from corners, and we can see no systematic relationship between the presence of dendrites and crystal size. More theoretical and experimental work is needed.

It is not clear why the secondary dendrite arms develop. Figures 3 and 4 show that they start developing near the end of the primary dendrite arms and that in many cases their external surfaces appear to be crystallographically controlled. Their inner surfaces and in some cases their outer surfaces do not appear to be crystallographically controlled.

One possible mechanism for their origin is that they develop after the primary dendrite tip penetrates, at least partially, the diffusion halo surrounding the crystal. Figure 4 indicates that there must be some statistical factor in their development, since the spacing of the secondary arms, while of the same order of magnitude, is neither constant nor variable in a uniform way.

From a purely geometric standpoint these experiments show, especially in Figure 4, that melt inclusions in olivine crystals are trapped primarily by the growth of secondary dendrite arms parallel to the original interface.

Comparison to natural hopper and dendritic morphologies

The development of the hopper and dendritic morphologies of the forsterite crystals in these experiments is similar to the development of generally similar morphologies of many natural phases. In most cases the interface breakdown of crystals in igneous rock is associated with edge effects rather than with random fluctuation on flat interfaces. (Whether this is due to macroscopic diffusional instability or random fluctuations at corners is not always clear.) The morphologies of many olivines in terrestrial and lunar basalt (Drever and Johnston, 1957; Donaldson *et al.*, 1975; Donaldson, 1976) are basically hopper-shaped with dendrite arms extending from the corners. Figure 2d shows a typical skeletal olivine phenocryst in glass from a mid-Atlantic ridge basalt. It is not hopper-shaped but does have dendrite arms

growing from corners. There is a kinematic wave on the lower right arm. Even the net dendrite olivines that grow in the margins of basalt pillows start their branching at corners (Kirkpatrick, 1979).

Other phases show generally similar morphologies. The arrowhead morphologies of chrome spinels and magnetites are due to development of dendrite arms from corners. The hopper and skeletal morphologies of pyroxene crystals (Walker *et al.*, 1976) are probably also due to edge or corner effects.

Note that the development of spherulites is a nucleation effect and unrelated to the development of hopper and dendritic morphologies (Keith and Padden, 1963; Kirkpatrick, 1979), although all form in response to composition gradients in the melt. The theory discussed here is not applicable to spherulites.

Interface melt composition

With the addition of effects associated with corners and reentrants, the melt compositions at the interfaces of forsterite crystals are in good qualitative agreement with theory. For a given crystal the difference between the melt compositions at the interface and far from the interface is least at corners and on dendrites and greatest in reentrants (Table 3). This is simply due to the geometrical effects of the melt volume to interface area ratio (Chernov, 1974).

For flat interface segments the increase in ΔMgO with increasing run time (Fig. 8) agrees well with the predictions of both Hopper and Uhlmann (1974) and Müller-Krumbhaar (1975).

The continual decrease in MgO at the interface with increasing value of the product of run time and cooling rate (Fig. 9) is also in good agreement with the theory of Müller-Krumbhaar. The reason the relationship is convex upward, rather than linear or concave upward as he shows it, is that the diffusion coefficients in the experiments are decreasing with decreasing temperature while he assumes a constant value. The upturn predicted by his theory is not observed. This may be because clinopyroxene nucleates before it can occur.

These results are also consistent with models which assume interface equilibrium, but the large CaO/MgO partition coefficients, their lack of systematic variation, the large variation for one crystal (Fig. 11), and the large variation in ΔMgO and ΔCaO even for a single crystal (Table 3) all argue for disequilibrium at the interface. The metastable olivine liquidus surface is not known, however, and it is possible (although we feel it unlikely) that something ap-

proximating interface equilibrium is being maintained.

Composition gradients in the melt

The composition gradients in the melt near the interfaces are in good qualitative agreement with the theory of Cooper and Gupta (1971). Figure 7 shows that the melt composition at the interface lies on the silica-rich side of the forsterite depletion line. Going away from the interface the compositions move towards the original bulk composition along a curved path that crosses or comes to the forsterite depletion line and then curves back towards the bulk composition. This is precisely the variation predicted by Cooper and Gupta. The point where the composition gradient crosses the forsterite depletion line is the mean composition of the liquid influenced by the forsterite growth.

It is not possible to analyze the quantitative applicability of the Cooper and Gupta theory to these experiments because the multicomponent exchange diffusion coefficients are not known and because the experiments were not isothermal. It is clear, however, that if we are to understand the growth of crystals from incongruently-melting compositions, we need values for this kind of diffusion coefficient, values which are in very short supply.

Occurrence of clinopyroxene and wollastonite

The first occurrence of clinopyroxene is suppressed more in these experiments than is the first occurrence of the liquidus phase in any other set of programmed cooling experiments in the same range of cooling rates. This is clearly associated with difficulties in nucleation and not slow growth, because the clinopyroxene growth rates are so high that if a small crystal were present it would rapidly fill the entire charge. This easy suppression of nucleation also occurs in microscope heating-stage experiments with the same composition (Kirkpatrick *et al.*, 1976).

The reason for the minimum in the clinopyroxene nucleation temperature at the intermediate cooling rates is not clear. The decrease from 10°/hr to 50°/hr can be explained kinetically—with increasing cooling rate the probability of nucleation of a crystal at a given temperature decreases because the time available decreases. Thus, a larger undercooling must be reached for nucleation to occur in a finite sample. This is the explanation usually given for similar variations observed in many sets of programmed cooling experiments (Walker *et al.*, 1976; Grove and Raudsepp, 1978).

The increase in the clinopyroxene nucleation temperature from 50°/hr to 300°/hr is unexpected and is the only such variation yet observed. The data in Table 4 indicate that heterogeneous nucleation on forsterite once a critical interface melt composition is reached cannot explain the variation. The interface compositions follow the cooling rate \times time relationship, and there is nothing unusual about the interface compositions in the runs quenched just prior to clinopyroxene nucleation. Neither is it likely that clinopyroxene is nucleating by a different mechanism in the higher cooling rate experiments. If this mechanism were available, it should be used at the slower cooling rates also. If this increase in nucleation temperature with increased cooling rate is found to be a common occurrence, more work on its origin may be justified.

The occurrence of wollastonite in these charges is the result of crystallization of forsterite and MgO-rich clinopyroxene, which leaves the melt enriched in CaO. Its occurrence between the clinopyroxene dendrite arms is a kinetic effect. Figure 7 shows that the liquid compositions before clinopyroxene forms are well within the clinopyroxene primary phase field. Once the clinopyroxene begins to grow, however, CaO builds up at the clinopyroxene–melt interface, and because the growth rate is so high it cannot diffuse far. Eventually wollastonite saturation (or supersaturation) is reached at the clinopyroxene interface and wollastonite crystallizes there.

Acknowledgment

These experiments were done in the experimental petrology laboratory at the NASA–Johnson Space Center in Houston. We are grateful to Gary Lofgren for allowing us the use of these facilities and Oscar Mullins for helping with the experiments. We are also grateful to Tim Grove and D. M. Henderson for their reviews of the manuscript. This work has been supported by NSF grants EAR 7682185 and EAR 7903923.

References

- Boyd, F. R., Finger, L. W., and Chayes, F. (1969) Computer reduction of electron probe data. *Carnegie Institution of Washington Year Book*, 67, 210–215.
- Chan, J. W. (1967) On the morphological stability of growing crystals. In H. S. Peiser, Ed., *Crystal Growth*, p. 681–690. Pergamon, Oxford.
- Chernov, A. A. (1974) Stability of faceted shapes. *Journal of Crystal Growth*, 24/25, 11–31.
- Cooper, A. R. and Gupta, P. K. (1971) Analysis of diffusion controlled crystal growth in multicomponent systems. In L. L. Hench and S. W. Freiman, Eds., *Advances in Nucleation and Crystallization in Glasses*, p. 131–140. American Ceramic Society, Columbus, Ohio.
- Donaldson, C. H. (1976) An experimental investigation of olivine

- morphology. *Contributions to Mineralogy and Petrology*, 57, 187–213.
- Donaldson, C. H., Usselman, T. M., Williams, R. J., and Lofgren, G. E. (1975) Experimental modeling of the cooling history of Apollo 12 olivine basalts. *Proceedings of the Lunar Science Conference*, 6th, 843–869.
- Drever, H. I. and Johnston, R. (1957) Crystal growth of forsteritic olivine in magmas and melts. *Transactions of the Royal Society of Edinburgh*, 63, 289–315.
- Elbaum, C. (1959) Substructures in crystals grown from the melt. In B. Chalmers and R. King, Eds., *Progress in Metal Physics*, Vol. 8, p. 203–204. Pergamon, London.
- Ghez, R. and Lew, J. S. (1973) Interface kinetics and crystal growth under conditions of constant cooling rate. *Journal of Crystal Growth*, 20, 273–282.
- Grove, T. L. and Raudsepp, M. (1978) Effects of kinetics on the crystallization of quartz normative basalt 15587: an experimental study. *Proceedings of the Lunar Science Conference*, 9th, 585–599.
- Grove, T. L. and Walker, D. (1977) Cooling histories of Apollo 15 quartz normative basalts. *Proceedings of the Lunar Science Conference*, 8th, 1501–1520.
- Hopper, R. W. and Uhlmann, D. R. (1974) Solute redistribution during crystallization at constant velocity and constant temperature. *Journal of Crystal Growth*, 21, 203–213.
- Jackson, K. A. (1958) Interface structure. In R. H. Doremus *et al.*, Eds., *Growth and Perfection of Crystals*, John Wiley and Sons, New York.
- Keith, H. D. and Padden, F. J. (1963) A phenomenological theory of spherulitic crystallization. *Journal of Applied Physics*, 34, 2409–2421.
- Kirkpatrick, R. J. (1974) Kinetics of crystal growth in the system $\text{CaMgSi}_2\text{O}_6$ – $\text{CaAl}_2\text{SiO}_6$. *American Journal of Science*, 274, 215–242.
- Kirkpatrick, R. J. (1975) Crystal growth from the melt—a review. *American Mineralogist*, 60, 798–814.
- Kirkpatrick, R. J. (1979) Processes of crystallization in pillow basalts, Hole 396B, DSDP Leg 46. *Initial Reports of the Deep Sea Drilling Project*, 46, 271–282.
- Kirkpatrick, R. J., Robinson, G. R., and Hays, J. F. (1976) Kinetics of crystal growth from silicate melts: anorthite and diopside. *Journal of Geophysical Research*, 81, 5715–5720.
- Lawrence, C. M. and Elwell, D. (1976) Growth stability of faceted crystals. *Journal of Crystal Growth*, 34, 316–318.
- Leven, E. M., Robbins, C. R., and McMurdie, H. F. (1964) *Phase Diagrams for Ceramists*. American Ceramic Society, Columbus, Ohio.
- Lofgren, G. (1974) An experimental study of plagioclase morphology. *American Journal of Science*, 264, 243–273.
- Lofgren, G., Donaldson, C. H., Williams, R. J., Mullins, O., and Usselman, T. M. (1974) Experimentally reproduced textures and mineral chemistry of Apollo 15 quartz normative basalts. *Proceedings of the Lunar Science Conference*, 5th, 549–567.
- Mullins, W. W. and Sekerka, R. F. (1964) Stability of a planar interface during solidification of a dilute binary alloy. *Journal of Applied Physics*, 35, 444–481.
- Müller-Krumbhaar, H. (1975) Diffusion theory for crystal growth at arbitrary solute concentration. *Journal of Chemical Physics*, 63, 5131–5138.
- O'Hara, S., Tarshis, L. A., Tiller, W. A., and Hunt, J. P. (1968) Discussion of interface stability of large facets on solution grown crystals. *Journal of Crystal Growth*, 314, 555–561.
- Roedder, E. and Weiblen, P. W. (1977) Compositional variation in late stage differentiates in mare lavas, as indicated by silicate melt inclusions. *Proceedings of the Lunar Science Conference*, 8th, 1767–1783.
- Tarshis, L. A. and Tiller, W. A. (1967) The effect of interface attachment kinetics on the morphological stability of a planar interface during solidification. In H. S. Peiser, Ed., *Crystal Growth*, p. 709–719. Pergamon, Oxford.
- Walker, D., Kirkpatrick, R. J., Longhi, J., and Hays, J. F. (1976) Crystallization history of lunar picrite basalt sample 12002: phase equilibrium and cooling rate studies. *Bulletin of the Geological Society of America*, 87, 646–656.
- Walker, D., Powell M. A., Lofgren, G. E., and Hays, J. F. (1978) Dynamic crystallization of a eucrite basalt. *Proceedings of the Lunar and Planetary Science Conference*, 9th, 1369–1391.
- Watson, E. B. (1979) Calcium content of forsterite coexisting with silicate liquid in the system Na_2O – CaO – MgO – Al_2O_3 – SiO_2 . *American Mineralogist*, 64, 824–829.

*Manuscript received, August 22, 1979;
accepted for publication, August 6, 1980.*